ELSEVIER

Available online at www.sciencedirect.com

ScienceDirect

Applied Mathematical Modelling 32 (2008) 99–111

APPLIED MATHEMATICAL MODELLING

www.elsevier.com/locate/apm

Revised particle growth model for supported metallocene catalyst co-polymerization

A. Alexiadis *, C. Andes

Max-Planck-Institut für Kohlenforschung, Kaiser-Wihlhelm-Platz 1, 45470 Mülheim an der Ruhr, Germany

Received 1 July 2005; received in revised form 1 November 2006; accepted 14 November 2006
Available online 21 March 2007

Abstract

In this paper, a revised version of the particle growth model (PGM) describing olefin co-polymerization with metallocene catalysts is proposed. The model is used to calculate the reaction rate of hexane–propylene co-polymerization under different operating conditions. Results are compared with experimental data obtained by calorimetric technique in order to validate the model. Good agreement between calculated and experimental results is shown.

Keywords: Modelling; Metallocene catalyst; Co-polymerization

1. Introduction

Microscopic analysis of silica supported metallocene catalysts [1] has shown the fragmentation mechanisms of the silica particle during the process of polymerization. Initially, an external polymeric film begins to grow all around the particle since the first active sites reached by the monomers are located on the external surface. The polymer covers the particle and starts to fill the internal silica pores, leading to a substantial diffusion limitation for the supply of new monomer to the internal active catalytic sites. The consequence of this phenomenon is a sudden drop in the reaction rate. With the ongoing polymerization, a shell-by-shell fragmentation of the SiO_2 particle from the surface to the centre occurs. This fragmentation is driven by the hydraulic forces of new polymer that is continuously produced at the accessible polymerization active centres. The ongoing fragmentation releases more and more active sites and reduces the diffusion limitation; therefore the macroscopic polymerization rate rises with the fragmentation of the particle. The final result is a completely fragmented particle with the original fragments totally dispersed into the polymeric matrix.

The initial peak in the reaction rate detected in experiments is a typical feature of this kind of systems and it has proven very hard to be model with traditional polymerization models.

* Corresponding author. Present address: Marie Curie Transfer of Knowledge Center for the Computational Sciences, Dept. of Mechanical and Manufacturing Engineering, University of Cyprus, 75 Kallipoleos St, PO Box 20537, 1678 Nicosia, Cyprus. Tel.: +357 22 892250; fax: +357 22 892254.
E-mail address: alexiadi@ucy.ac.cy (A. Alexiadis).

0307-904X/$ - see front matter
doi:10.1016/j.apm.2006.11.006

Nomenclature

D_l	diffusion coefficient in the macro-particle ($m^2\ s^{-1}$)
D_s	diffusion coefficient in the micro-particle ($m^2\ s^{-1}$)
k	kinetic constant ($m^3\ mol^{-1}\ s^{-1}$)
k_s	mass transfer coefficient in the external film ($m\ s^{-1}$)
$[M]_i$	i-monomer concentration in the macro-particle ($mol\ m^{-3}$)
$[M]_b$	i-monomer concentration in the bulk ($mol\ m^{-3}$)
r_l	radial variable along the macro-particle radius (m)
R_l	macro-particle radius (m)
R_s	macro-particle radius (m)
R_p	polymerization rate per catalyst volume ($mol\ m^{-3}\ s^{-1}$)
t	time (s)
T_{REF}	reference temperature (K)
v_H	apparent hexene reaction rate ($mol\ m^{-3}\ s^{-1}$)
v_P	apparent propylene reaction rate ($mol\ m^{-3}\ s^{-1}$)
v_{TOT}	apparent total reaction rate, $=v_P + v_H$ ($mol\ m^{-3}\ s^{-1}$)
w_{Zr}	weight percentage of Zr in the particle
x_H	hexene mole fraction
x_P	propylene mole fraction, $=1 - x_H$
[Zr]	total zirconium concentration in reactor ($mol\ m^{-3}$)

Greek letters

γ	polymerization ratio
ε	void macro-particle fraction
φ	micro-particle growth factor defined in Eq. (7)
ρ_{cat}	catalytic particle density ($kg\ m^{-3}$)
ρ_{pol}	average polymer density ($kg\ m^{-3}$)

Superscripts

0	initial condition ($t = 0$)
1	active catalytic site type 1
2	active catalytic site type 2
i	i-monomer

Subscripts

g	relative to transformation reaction
H	hexene
i	i-monomer
p	relative to propagation reaction
P	propylene
t	relative to transformation β-transfer reaction
r	relative to reactivation reaction
d	relative to deactivation reaction

Probably the most known model describing polymerization in supported catalysts is the multigrain model (MGM) [2]. It considers the particle as a macro-particle divided into many micro-particles (the fragments). The polymer grows on the surface of the micro-particles, which expand their volume and, consequently, make the macro-particle expand as well. This model supposes that the macro-particle is completely fragmented from

the beginning. It gives good results in the case of Ziegler–Natta catalysts where the previous assumption holds but it is not very accurate in the case of metallocene catalysts where the fragmentation happens with a shell-by-shell process.

A model that improves the MGM is the particle growth model (PGM) [3]. This model assumes a shell-by-shell fragmentation where each fragmented layer behaves as the MGM. However, it ignores diffusion inside the non-fragmented part and its validity is restricted only to the cases where the limiting phenomenon is the monomer diffusion into the fragmented part.

A two region model (TRM) has been introduced in [4,2] in order to take into account the non-fragmented zone. This model divides the particle in two regions: the fragmented part and the solid core, which are considered as separate media with different physical proprieties. This model overcomes some of the limits of the PGM but it does not model the phenomenon of fragmentation and it fails to predict the initial peak, which appears in the reaction rate profile.

In [5] a model that combines some of the properties of the PGM and of the TRM has been proposed. This model correctly describes the initial peak of reaction rate and gives a good agreement with experimental data. However, contrary to previous models, its application has been limited to the homo-polymerization case (where only one type of monomer is considered) and never extended to co-polymerizations (where different monomers are taken into account). In this paper, the model is reformulated and adapted to homo-polymerizations and results compared with experiments.

2. Mathematical modelling

Particles are considered to be spherical and fragmentation happens shell-by-shell from the surface to the centre. In this way it is possible to identify two regions: a fragmented zone that extends from the surface to the fragmentation front and an unfragmented core that extends from the fragmentation front to the centre. The particle is fragmenting and, as consequence, the fragmentation front is moving from the surface to the centre. When it reaches the centre the particle is assumed completely fragmented. The fragments, generated during the fragmentation process, are assumed spherical as in the 'multigrain model' (MGM) (see [6]).

Two kinds of particles are identifiable (Fig. 1): macro-particles (the original pellet) and micro-particles (the resultant fragments). The polymerisation process begins at the surface and in the pores of the micro-particle and a thicker and thicker layer of polymer forms all around the micro-particles. The macro-particle is consequently growing because the micro-particles are growing as well.

Diffusion of monomer into the fragmented part is a two steps process. First the monomer diffuses in the macro-particle (macro-scale), then into the polymeric layer of the micro-particle (micro-scale), finally it reaches the catalytic active sites and, according to the kinetic scheme, it reacts (molecular scale).

In [5], the original particle growth model (PGM) was improved by taking into account diffusion and reaction in the unfragmented core. In this region only two scales are involved (macro and molecular) because there are no fragments (micro-particles).

The macro-particle is, consequently, divided in two parts: the unfragmented core ($\xi < \xi_F$ where ξ is the dimensionless radial coordinate and ξ_F the dimensionless fragmenting radius) and the fragmented part ($\xi > \xi_F$) composed of many micro-particles. Micro-particles are composed of an original fragment (R_0) and a polymeric layer ($R - R_0$) growing all around it.

After some mathematical manipulation (see [1,3,5,7]) it is possible to write the governing equation (here in dimensionless form) in the fragmented and unfragmented part for the monomer dimensionless concentrations (ψ_i).

In [6] it is possible to find a more detailed description of the MGM, the basis for the fragmented part modelling. Good references for understanding the origin of PGM and the differences between PGM and MGM are found in [3,7]. In [5], the revised PGM model (including solid core modelling) is presented.

Here a further evolution of the model, from homo- to co-polymerization is proposed.

Although heat balance was also taken into account in [5], it is not presented here because, for all the cases studied in this paper, the computed temperature profiles inside the particle were almost constant.

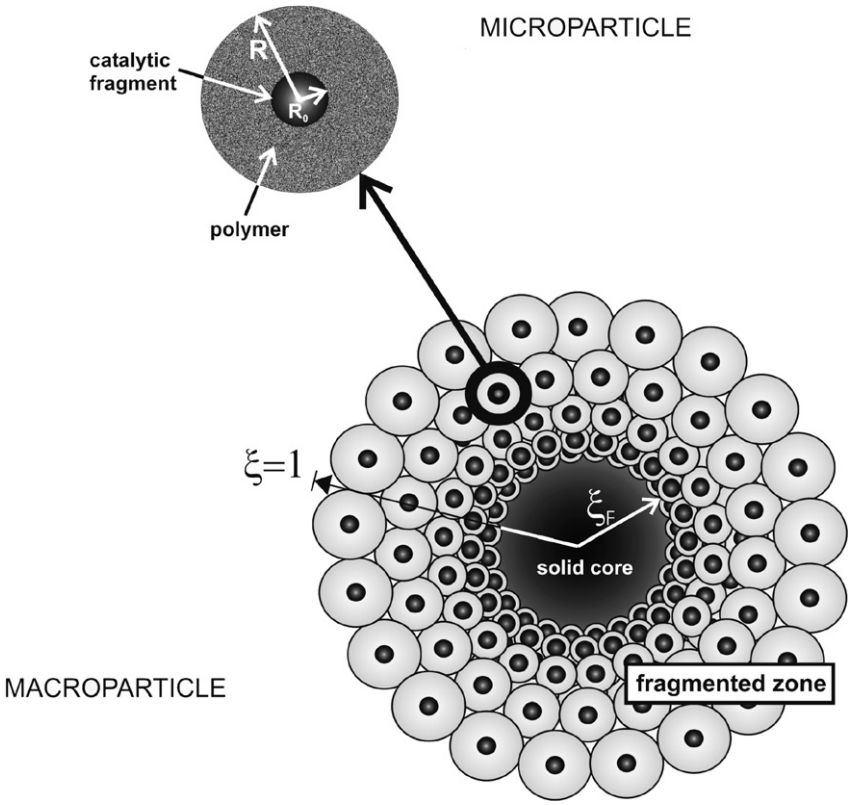

Fig. 1. Schematic representation of micro- (left) and macro- (right) particles as used in the model.

The model assumes that both the fragmented part and the solid core are spherical. This is not, of course, the case of real particles. Videomicroscopic analysis [8] shows, however, that in many cases particles can be assumed roughly spherical.

2.1. Fragmented zone

Mass balance (fragmented part $\xi > \xi_F$):

$$\varepsilon \frac{\partial \psi_i}{\partial \tau} = \frac{1}{\xi^2} \frac{\partial}{\partial \xi} \left(\varepsilon \delta_i \xi^2 \frac{\partial \psi_i}{\partial \xi} \right) - \psi_i Da_i. \tag{1}$$

Eq. (1) is written in dimensionless form (see Table 1 for the significance of dimensionless number used). The first term on the left hand side of Eq. (1) represents the local accumulation of the monomer i in the fragmented zone, the first term on the right hand side the diffusion and the second term the dimensionless chemical reaction rate.

The dimensionless parameter δ_i is the ratio between the diffusion coefficient of the i-monomer and the 1-monomer chosen as basis ($\delta_1 = 1$, $\delta_2 = D_l^{i=2}/D_l^{i=1}$, $\delta_3 = D_l^{i=3}/D_l^{i=1}$, etc.).

The micro-particle equations do not appear directly here but they enter, after some mathematical manipulation [3,6,7], in the Damköhler term of Eq. (1).

Boundary conditions (external radius $\xi = 1$):

$$\xi = 1, \quad \frac{\partial \psi_i}{\partial \xi} = Sh_i(1 - \psi_i). \tag{2}$$

The unfragmented core modelling is considered a classical (without fragmentation) catalytic particle where reactions take place on the surface of its internal pores [9].

Table 1
Dimensionless numbers

	Symbol	Formula
Dimensionless monomer conc.	ψ_i	$[\mathrm{M}]_i/\sum_{j=1}^{i_{\max}}[\mathrm{M}]_\mathrm{b}^j$
Dimensionless radial coordinate[a]	ξ	r_l/R_l
Dimensionless diffusion	δ_i	$D_l^i/D_l^{i=1}$
Dimensionless time	τ	$tR_l^2/D_l^{i=1}$
Sherwood number	Sh_i	$k_\mathrm{s}R_l/D_l^i$
Damköhler group (fragment. zone)	Da_i	$\dfrac{R_l^2R_\mathrm{P}^i}{D_l^{i=1}\sum_{j=1}^{i_{\max}}[\mathrm{M}]_\mathrm{b}^j}\dfrac{1-\varepsilon}{\varphi^3}$
Damköhler group (core)	Da_i^*	$\dfrac{R_l^2R_\mathrm{P}^i}{D_l^{i=1}\sum_{j=1}^{i_{\max}}[\mathrm{M}]_\mathrm{b}^j}$

[a] Note that R_l is the actual radius of the macro-particle and it varies with time.

2.2. Solid core

Mass balance (core $\xi < \xi_\mathrm{F}$):

$$\varepsilon\frac{\partial\psi_i}{\partial\tau} = \frac{1}{\xi^2}\frac{\partial}{\partial\xi}\left(\varepsilon X_i\xi^2\frac{\partial\psi_i}{\partial\xi}\right) - \psi Da_i^*. \tag{3}$$

The physical significance of the different terms in Eq. (3) is the same of Eq. (1) with the difference that, in this case, accumulation, diffusion and chemical reaction occur in the solid core instead of the fragmented part.

The dimensionless number X_i is the ratio between i-monomer diffusion before and after fragmentation.

Boundary conditions (particle centre $\xi = 0$):

$$\xi = 0, \quad \frac{\partial\psi_i}{\partial\xi} = 0. \tag{4}$$

Interaction between fragmented zone and core ($\xi = \xi_\mathrm{F}$):

$$\left.\frac{\partial\psi_i}{\partial\xi}\right|_{\xi_\mathrm{F}^+} = X_i\left.\frac{\partial\psi_i}{\partial\xi}\right|_{\xi_\mathrm{F}^-}. \tag{5}$$

Initial conditions ($\forall\xi$):

$$\tau = 0, \quad \psi_i = 0. \tag{6}$$

A further condition, which has to be taken into consideration, is the initial distribution of active sites in the catalytic pellet. In the case under study, it was assumed uniform since it is not completely known (for the same reason all the initial Zr was considered active). See also [1] with EDX-data.

A parameter called particle-growing factor (φ) is introduced for simulating fragmentation and evolution of the fragmentation front

$$\varphi = \frac{R_\mathrm{s}}{R_\mathrm{s}^0}. \tag{7}$$

This parameter expresses the idea of micro-particles growth and depends on the polymer deposited on the surface. Fragmentation was taken into account by means of a critical φ for the first time in [3].

When the polymer layer has grown around the particle then $\varphi > \varphi_\mathrm{cr}$ and the particle is considered locally fragmented and it is free to expand [6].

Often two parameters are used in the modelling: one for the first layer (φ_cr) and another one for the rest of the particle (φ_cr). This solution was first adopted in [3] in order to take into account the fact that after the fragmentation starts the pellets are more fragile. These parameters are handled as physical properties of the particle and were inferred from experimental data [5,10].

3. Reaction scheme

In Eqs. (1) and (3) the chemical reaction are included in the Damköhler numbers Da_i and Da_i^*. The intrinsic reaction rate R_P^i is incorporated in the Damköhler number and depends on the reaction involved.

Table 2 shows the kinetic scheme used for describing the reaction involved [3,7], i_{max} is the number of i-monomers considered. Two kinds of active sites are present (types 1 and 2). Reaction with Al(I-Bu)$_3$ (TIBA), causes the active site transformation from type 1 to type 2. Both sites have propagation reactions of the polymer chain P_n, β-hydride chain transfer forming a dead polymer chain D_n and a temporary free site PH, reactivation of those sites by reaction with the monomer M_i and, finally, bimolecular sites deactivation giving origin to death sites C_d. Kinetic constants values for pure hexane and pure propylene are reported in Table 3.

3.1. Co-polymerization effects in C_3H_6 and C_6H_{12} mixtures

In the case of co-polymerization the scheme of reaction reported in Table 2 must be applied to all monomers studied. Nevertheless the presence of a slower reacting monomer can affect the kinetics of another monomer.

In this paper the model will be validated through experimental data coming from binary ($i_{max} = 2$) propylene–hexene co-polymerization [10]. In this case, small quantities of C_6H_{12} are sufficient to slow down dramatically the global reaction rate (Fig. 2).

A small quantity of hexene ($x_H = 0.007$) causes the reaction rate to drop considerably. Propylene does not have the same effect as hexene. Fig. 2 compares v_{TOT}, which is the global "overall" reaction rate. It is called overall because is not the intrinsic molecular reaction rate R_P but the apparent one, which depends on all the involved phenomena (diffusion, fragmentation, etc.).

Table 2
Chemical kinetic scheme

Transformation	$P_n^1 + TIBA \rightarrow P_n^2$	k_g	$n = 0,\ldots,\infty$
Propagation	$P_n^1 + M_i \rightarrow P_{n+1}^1$	$(k_p^1)_i$	$n = 0,\ldots,\infty;\ i = 1,\ldots,i_{max}$
	$P_n^2 + M_i \rightarrow P_{n+1}^2$	$(k_p^2)_i$	$n = 0,\ldots,\infty;\ i = 1,\ldots,i_{max}$
β-Transfer	$P_n^1 \rightarrow PH^1 + D_n^1$	k_t^1	$n = 1,\ldots,\infty$
	$P_n^2 \rightarrow PH^2 + D_n^2$	k_t^2	$n = 1,\ldots,\infty$
Reactivation	$PH^1 + M_i \rightarrow P_1^1$	$(k_r^1)_i$	$i = 1,\ldots,i_{max}$
	$PH^2 + M_i \rightarrow P_1^2$	$(k_r^2)_i$	$i = 1,\ldots,i_{max}$
Deactivation	$P_n^1 + P_m^1 \rightarrow 2C_d + D_n^1 + D_m^1$	k_d^1	$n,m = 0,\ldots,\infty$
	$P_n^2 + P_m^2 \rightarrow 2C_d + D_n^2 + D_m^2$	k_d^2	$n,m = 0,\ldots,\infty$

Table 3
Kinetic constant used for simulations

	C_3H_6	C_6H_{12}
k_g [cm^3 mol^{-1} s^{-1}]	9.8×10^4	9.8×10^4
k_p^1 [cm^3 mol^{-1} s^{-1}]	2.0×10^8	1.3×10^7
k_p^2 [cm^3 mol^1 s^{-1}]	1.3×10^7	1.0×10^5
k_t^1 [s^{-1}]	1.5×10^5	1.0×10^5
k_t^2 [s^{-1}]	5.0×10^4	5.0×10^4
k_r^1 [cm^3 mol^{-1} s^{-1}]	2.8×10^5	5.0×10^2
k_r^2 [cm^3 mol^{-1} s^{-1}]	1.5×10^6	5.0×10^2
k_d^1 [cm^3 mol^{-1} s^{-1}]	2.6×10^7	5.2×10^{12}
k_d^2 [cm^3 mol^{-1} s^{-1}]	3.4×10^7	6.8×10^{12}

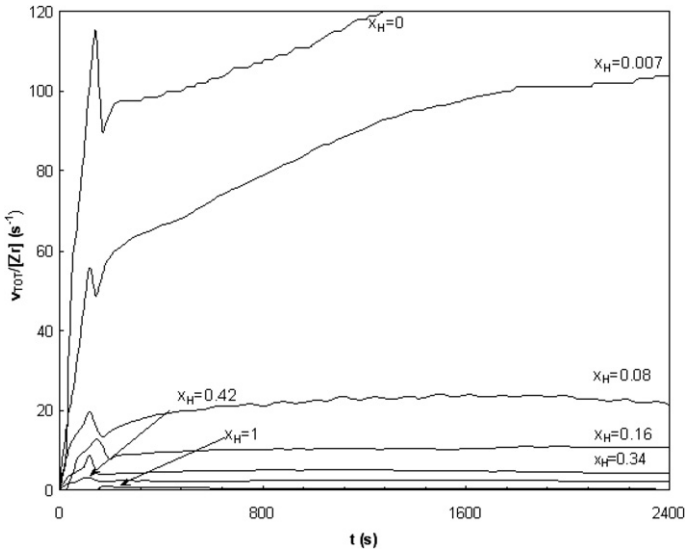

Fig. 2. Experimental data of global reaction rate (divided by the total zirconium concentration [Zr]) coming from hexene–propylene bulk co-polymerization at different x_H (hexene mole fraction) values.

Table 4
Ratios between propylene kinetic constants in case of homo-polymerization and hexene–propylene co-polymerization vs. hexane molar fraction

x_H	γ
0	1
0.007	0.79
0.08	0.55
0.16	0.35
0.32	0.09
0.42	0.05
1	0

The presence of bigger and slower reacting monomers (C_6H_{12}) disturbs the reaction of the smaller and faster reacting monomers (C_3H_6). The constants $k_p^{1,2}$ and $k_r^{1,2}$ (see Table 3) related to the C_3H_6 reaction, in particular, are affected by the hexane and their values decrease with the C_6H_{12} concentration. The analysis of experimental data [10] shows that the hexane concentration influences the four propylene kinetic constants $k_p^{1,2}$ and $k_r^{1,2}$ approximately in the same way. The ratios γ between $k_p^{1,2}$ and $k_r^{1,2}$ for pure propylene homo-polymerizations and for hexane–propylene co-polymerizations at different x_H are reported in Table 4. The parameter γ can be used to find the propylene kinetic constants in the mixture as function of the hexane concentration.

$$k_{p,r}^{1,2}(x_H) = \gamma(x_H) k_{p,r}^{1,2}(0) \quad (0 \leqslant \gamma \leqslant 1). \tag{8}$$

Finally, it has to be taken into account the fact that in liquid olefins the polymer can be very soluble. Here, it was assumed that the number of pellets in the reactor is very high and saturation occurs very quickly. Details about the structure of the particles before, during and after polymerization can be found in [11–13].

4. Short description of experiments [10]

The catalyst system employed for this study was $Me_2Si[R^1Ind]_2ZrCl_2/MAO/SiO_2$, supplied by industry. $Al(^iBu)_3$ was used as a scavenger for all reactions. 1-Hexene was dried using $NaAlEt_4$ and distilled directly

before use. Propene (99.95%) was obtained from Messer Griesheim Gmbh. and used without further purification.

All polymerisations were carried out in a 1.8 L high pressure steel reactor (HP 60) using the Mettler RC1 reaction calorimeter. All reactions were carried out in isothermal mode at 60 °C using an anchor stirrer at 250 rpm. An externally controlled bath (62 °C) maintained the temperature of the reactor lid and the injector port, limiting heat loss and heating the catalyst solution to the reaction temperature before injection.

1-Hexene and Al(^{i}Bu)$_3$ (1.5 mL) were added directly to the clean and dry reactor using Schlenck techniques. Propene was then condensed in the reactor at approximately 0 °C to give a final monomer volume of 1 L. The amount of each monomer added is varied depending on the desired 1-hexene mole ratio. The bulk monomer mixture was then heated to 60 °C. The total pressure of the reactor depends on the composition of the monomers, due to the difference in the vapour pressure of the monomers. A solution of the catalyst suspended in 7 mL heptane and heated to 62 °C was injected into the reactor under Ar pressure. Another 5 mL of heptane, also heated to 62 °C, was then immediately injected through the injector port to rinse any remaining catalyst particles into the reactor. The polymerisation was stopped by the addition of MeOH to the reactor. For further details see [10].

5. Results

5.1. Pure C_3H_6 and pure C_6H_{12}

Modelling of 'pure' ($x_H = 0$ and $x_H = 1$) cases does not present any problem and follows the work done in [5]. The values of the kinetic constants were derived by fitting data from experiments with pure propylene and hexene [5,10]. In Fig. 3a and b it is possible to see the comparison between numerical results and experimental data of pure propylene ($x_H = 0$) and pure hexene ($x_H = 1$). Fig. 3a and b shows that the pure hexene chemical

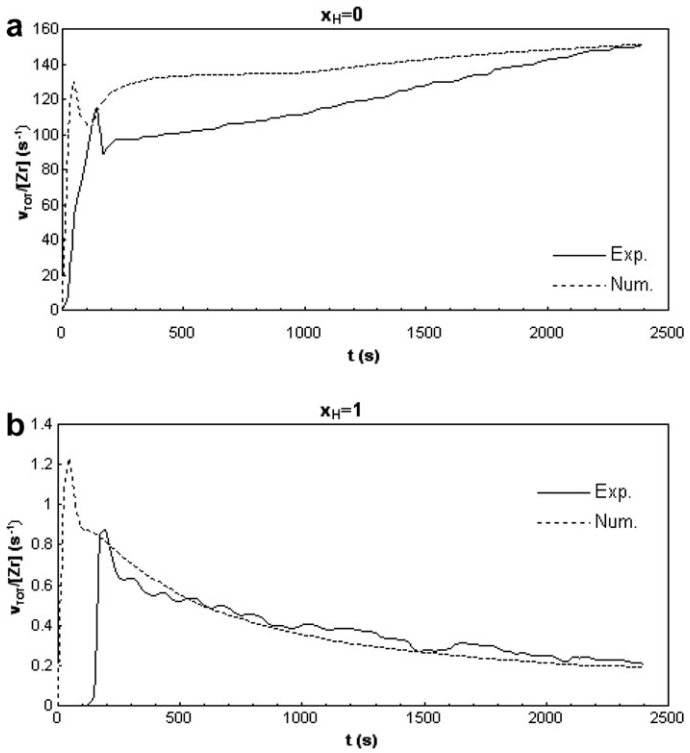

Fig. 3. Comparison between numerical results and experimental data of global reaction rate (divided by the total zirconium concentration [Zr]) of bulk polymerization of pure propylene ($x_H = 0$) (a) and pure hexene ($x_H = 1$) (b).

Table 5
Parameters used for simulations (between square parenthesis are quoted the reference from which the values are taken)

ρ_{pol} [g cm^{-3}] [3,7]	0.9	
[Zr] [mol cm^{-3}]	Variable [10]	
Boundary layer correlation [15]	Ranz-Marshall	
ρ_{cat} [g cm^{-3}] [3,7,15]	2.25	
R_s^0 [μm] [3,6,7]	0.01	
w_{Zr} [10]	0.27	
ε [3,7]	0.25	
R_l^0 [μm] [5]	25	
φ_{cr} [5]	1.8	
φ_{cr} [5]	1.9	
	C_3H_6	C_6H_{12}
D_s [m^2 s] [3,7,15]	4.0×10^{-7}	1.0×10^{-8}
D_l [m^2 s] [3,7,15]	1.4×10^{-6}	1.5×10^{-8}
X_i [5]	0.01	0.09

reaction rate decreases with time while the pure propylene rate increases. The reason is that the hexene diffusivity in the macro-particle is two orders of magnitude lower than the diffusivity of propylene and the hexene deactivation kinetic constants are much higher than the analogous propylene constants. This circumstance has as a consequence a low concentration of hexane at the catalyst surface, which, in turn, favours deactivation in the reaction scheme shown in Table 2.

The kinetic constants (Table 3) are the same as in [5] considered the different T_{REF} (here $T_{REF} = 60$ °C, in [5] $T_{REF} = 40$ °C). In Table 5 are listed the physical parameter used in these and the following numerical simulations.

5.2. C_3H_6 /C_6H_{12} mixtures

When propylene and hexene are considered together, some of the kinetic constants of propylene ($k_p^{1,2}$ and $k_r^{1,2}$) have to be multiplied by the parameter γ according to Eq. (8). In this way, it is possible to compute numerical data of propylene–hexene mixtures at different concentrations. In Fig. 4 comparisons between experimental data and numerical results for different values of x_H are reported.

The comparison between experimental data and numerical computation is usually acceptable. Some differences can be seen in the initial phase, where a peak is present in all cases considered. In the first steps of polymerization, the polymer is formed inside the unfragmented particle pores. This growing polymer limits further monomer diffusion; consequently the reaction rate diminishes (the peak) until fragmentation starts. From this point on, diffusion inside the fragments is easier and the reaction continues again.

Figs. 3 and 4 show that the peaks in the model are constantly anticipated with respect to the experimental cases. The reason of this observed phenomenon is still not completely understood. One limit of the PGM is that the model assumes only spherical particles, while real particles are not perfectly spherical and fragmentation does not occur symmetrically along the particle radius: it is possible that this circumstance can play a role in the peak anticipation described above. Furthermore, it must be noticed that the experimental data originate from calorimetric methods [10] and a certain delay in the record of the data can be expected.

6. Discussion

The comparison between experimental data and numerical results allows validation of the model; once the model is valid it is possible to use it to look at those parameters that are not evident during experiments. Experimental data are based on calorimetric procedures [14] that work thanks to the fact that both reactions have a ΔH of approximately 25 kcal mol^{-1}. This method cannot distinguish between heat coming from propylene or hexene polymerization and only total reaction rates are derived in experiments.

The model can be used for separating v_H and v_P from v_{TOT}, additionally it can also allow a deeper look into the particles and the concentration profiles of propylene and hexene inside the catalytic particle. Fig. 5, for

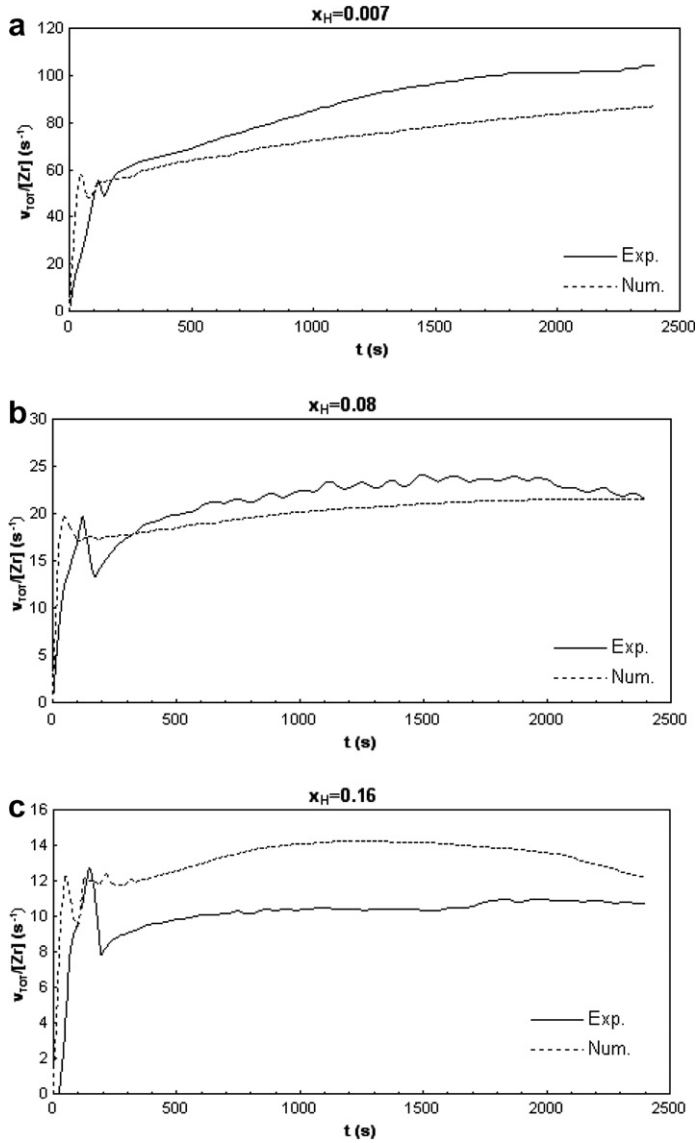

Fig. 4. Comparison between numerical results and experimental data of global reaction rate (divided by the total zirconium concentration [Zr]) of bulk hexene–propylene co-polymerization at different hexene mole fractions. (a) $x_H = 0.007$, (b) $x_H = 0.08$, (c) $x_H = 0.16$, (d) $x_H = 0.34$ and (e) $x_H = 0.42$.

instance, shows that between $x_H = 0.42$ and $x_H = 0.34$ the situation changes completely. At $x_H = 0.42$ the hexane reaction rate v_H is lower than v_P but comparable. If x_H decreases to 0.34, v_H is almost negligible compared to v_P. Nevertheless it has an indirect influence because a small quantity of hexene is enough to slow down the propylene reaction.

Considering the monomer concentration inside the particle, the hexene concentration is often higher than the propylene concentration (Figs. 6 and 7). Fig. 6 represents the dimensionless propylene concentration (ψ_P) in the particles at different times for the case $x_H = 0.34$ (Figs. 4d and 5b). Each curve represents the dimensionless concentration at a different time. Those curves are intersected by the fragmentation front line. The part of the curve, which lies right of the intersection point is fragmented, while the other part is not yet fragmented. In Fig. 6, the curve representing the concentration profile at $t = 1050$ s intercepts the fragmentation line at $\xi = 0.158$. This means that after 1050 s of polymerization the particle is fragmented until a

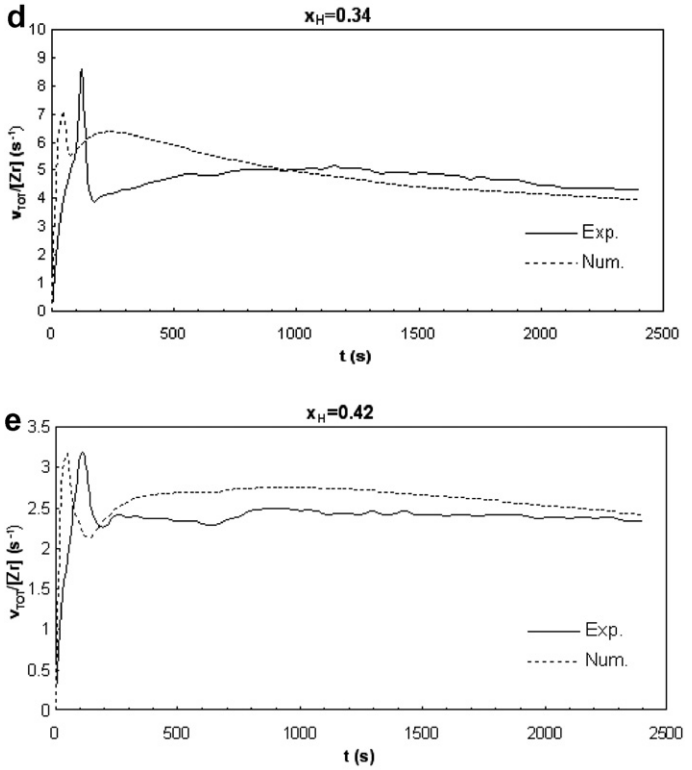

Fig. 4 (*continued*)

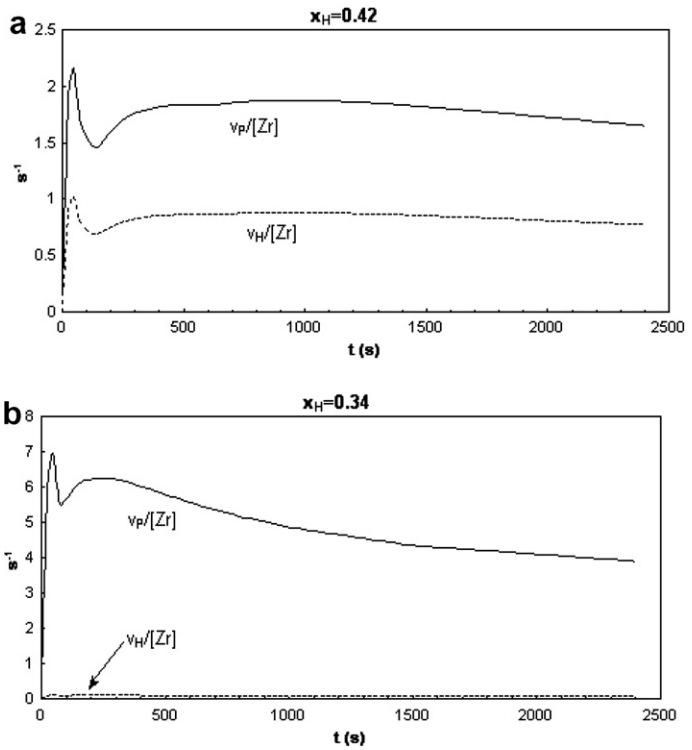

Fig. 5. Numerical computed profiles of propylene reaction rate (v_P) and hexene reaction rate (v_H) (divided by the total zirconium concentration [Zr]) of bulk co-polymerization for $x_H = 0.42$ (a) to $x_H = 0.34$ (b).

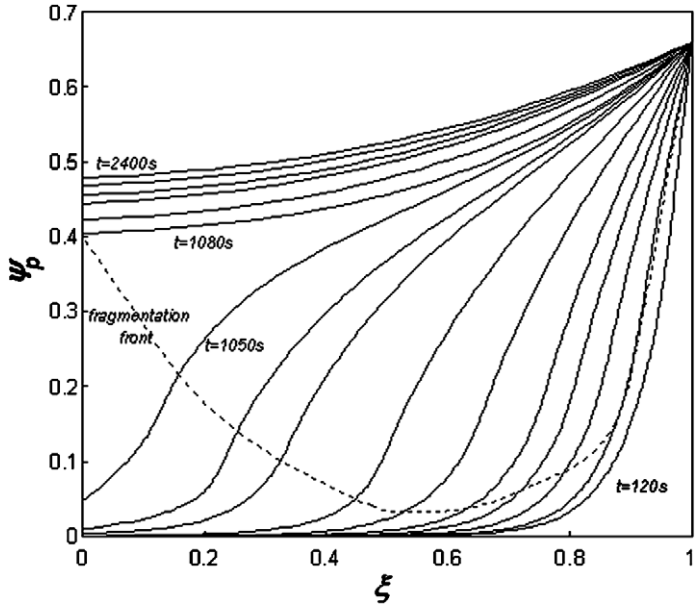

Fig. 6. Propylene dimensionless concentrations ψ_P vs. dimensionless diameter ξ, computed, at different time t, inside the macro-particle during the bulk hexene–propylene co-polymerization in case of $x_H = 0.34$.

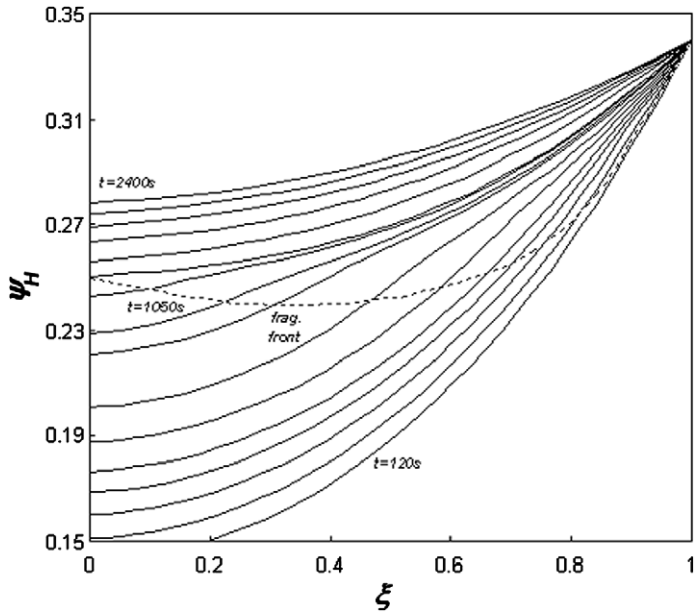

Fig. 7. Hexene dimensionless concentrations ψ_H vs. dimensionless diameter ξ, computed, at different time t, inside the macro-particle during the bulk hexene–propylene co-polymerization in case of $x_H = 0.34$.

dimensionless diameter of 0.158 while it is not fragmented inside this point. After 1080 s the particle is completely fragmented.

It is interesting to note the phase of complete fragmentation of the particle. It happens (for the case considered in Figs. 6 and 7, computed at $x_H = 0.34$) after 1080 s of polymerization. In Fig. 6 we can see clearly the different behaviour and diffusion between the unfragmented and the fragmented part. In the more compact

central core, it is harder for propylene to diffuse and concentrations are low. After the particle fragmentation the monomer can fill the cracks which are forming, diffusion becomes easier and concentration higher.

Fig. 7 is the equivalent of Fig. 6 for the dimensionless hexene concentration (ψ_H). Before complete fragmentation, the hexene concentration in the particle is higher than propylene. In fact the hexene reaction rate is much slower than the propylene one (see Fig. 5b), consequently it is the controlling factor with respect to diffusion. Seen in a different way, hexene has time to diffuse into the particle because its reaction rate is smaller.

7. Conclusion

The goal of this paper is to extend the particle growth model (PGM), proposed in revised form in [5]. Until now, this model has been tested only for homo-polymerization, but here it is extended to the case of co-polymerization. Interaction among co-monomers must be considered. In this work, hexane–propylene mixtures are studied. The hexene molecules, bigger and slower to react, interfere with the propylene access to the active sites and slow down the reaction rate. This effect is taken into account in the model through the polymerization ratios γ. Good agreement between calorimetric experimental data and numerical results computed with the model proposed in this paper are shown.

References

[1] S. Knoke, F. Korber, G. Fink, B. Tesche, Early stages of propylene bulk phase polymerization with supported metallocene catalysts, Macromol. Chem. Phys. 204 (2003) 607.
[2] E.J. Nagel, V.A. Kirillov, W. Harmon Ray, Prediction of Molecular-weight distributions for high-density polyolefins, Ind. Eng. Chem. Prod. Res. Dev. 19 (1980) 372.
[3] F. Bonini, V. Fraaije, G. Fink, Propylene polymerization through supported metallocene MAO catalysts kinetic-analysis and modeling, J. Polym. Sci. A 33 (1995) 2393.
[4] M.A. Ferrero, M.G. Chiovetta, Catalyst fragmentation during propylene polymerization. 1. The effects of grain-size and structure, Polym. Eng. Sci. 27 (1987) 1436.
[5] A. Alexiadis, C. Andes, K. Hauschild, M. Bochman, G. Fink, Mathematical modeling of homopolymerization on supported metallocene catalysts, Macromol. Mater. Eng. 289 (2004) 457.
[6] R.A. Hutchinson, C.M. Chen, W.H. Ray, Polymerization of olefins through heterogeneous catalysis. 10. Modeling of particle growth and morfology, J. Appl. Polym. Sci. 44 (1992) 1389.
[7] C. Przybyla, B. Weimann, G. Fink, Influence of the particle size of silica support on the kinetics and the resulting polymer properties at the polypropylene polymerization with heterogeneous metallocene catalyst; Part II: Development of a model as well as a mathematical simulation, in: W. Kaminsky (Ed.), Metallorganic Catalysts for Synthesis and Polymerization, Springer, Berlin, 1999, pp. 333–346.
[8] D. Ferrari, S. Knoke, B. Tesche, G. Fink, Microkinetic videomicroscopic analysis of the olefin-copolymerization with heterogeneous catalysts, Macromol. Symp. 236 (2006) 78–87.
[9] K.R. Westerterp, W.P.M. Van Swaaij, A.A.C.M. Beenackers, Chemical Reactor Design and Operation, third ed., John Wiley & Sons, 1988.
[10] C. Andes, Reaction calorimetry to study the copolymerization of 1-hexene and liquid propene, in: Meetings of the European Research Network: New Polyolefin Materials via Metal Catalyzed Copolymerizations, 26–28 September 2003, Anacapri, Italy.
[11] S. Knoke, D. Ferrari, B. Tesche, G. Fink, Microkinetic videomicroscopic analysis of olefin polymerization with a supported metallocene catalyst, Angew. Chem., Int. Ed. 42 (2003) 5090.
[12] J. Zechlin, K. Hauschild, G. Fink, Silica supported metallocene/MAO-systems: comparison of the polypropylene growth during bulk phase polymerization with slurry phase experiments, Macromol. Chem. Phys. 201 (2000) 597.
[13] J. Zechlin, B. Steinmetz, B. Tesche, G. Fink, Development of a refined poly(propylene) growth model for silica supported metallocene catalyst systems, Macromol. Chem. Phys. 201 (2000) 515.
[14] F. Korber, K. Hauschild, M. Winter, G. Fink, Reaction calorimetric investigation of the propylene slurry phase polymerization with a silica-supported metallocene/MAO catalyst, Macromol. Chem. Phys. 202 (2001) 3323.
[15] S. Floyd, K.Y. Choi, T.W. Taylor, W.H. Ray, Polymerization of olefins through heterogeneous catalysis. 3. Polymer particle modeling with an analysis of intraparticle heat and mass-transfer effects, J. Appl. Polym. Sci. 32 (1986) 2935.